Multi-Environment Probability Density Function Method for Modeling Turbulent Combustion Using Detailed Chemistry

Qing Tang, Jinliang Ma, Michael Bockelie, Reaction Engineering Int., Salt Lake City, UT
Wei Zhao, United Technology Research Center, East Hartford, CT
Rodney O. Fox, Iowa State University, Ames, IA

Introduction

One of the most important issues to address in turbulent combustion calculations is the intense nonlinear interaction between fluid mixing and finite-rate chemistry. In combustion processes which are characterized by fast chemistry, use of the flamelet model (Peter, 1984) or conditional moment closure (CMC) (Bilger, 1993) based on a conserved scalar is known to be quite accurate in making qualitative as well as quantitative predictions. However, these methods may not be viable in slow chemistry regimes such as the formation and destruction of NOx. The flamelet model requires the specification of a scalar dissipation rate and assumes the shape of the PDF at the sub-grid level. The first-order CMC model ignores any fluctuations about the conditional mean. The transported PDF method (Pope, 1985), on the other hand, computes the joint PDF in terms of a set of delta-functions. The principal advantage of the method is that the chemical reaction appears in closed form in the PDF equations. As a consequence, realistic combustion chemistry can be incorporated without the need for closure approximations pertaining to reaction. Therefore, PDF methods are able to accurately describe turbulent-chemistry interactions in turbulent flames. Other processes – notably molecular diffusion – have to be modeled. The transport joint PDF equation is multi-dimensional and cannot be solved using Eulerian grid techniques. Recent PDF calculations using particle based Monte-Carlo schemes with realistic chemistry show good agreement with experimental results (Tang et al., 2000; Xu and Pope, 2000; Lindstedt et al., 2000; Raman et al., 2004). However, the handling of a large number of Lagrangian particles along with detailed chemistry can be computationally prohibitive in practical flow configurations.

Starting from the PDF transport equation, the multi-environment PDF (MEPDF) model can be derived. The model is based on a presumed form for the joint composition PDF and retains many of the desirable properties of the transport PDF method including the ability to treat the chemical source term exactly. Moreover, the computational cost of solving the MEPDF model for the same number of scalars is only a fraction of the cost of transported PDF simulation (Wang and Fox, 2004). Recently this method has been adapted into large eddy simulations (LES) as a sub-grid model for simulating gas phase combustion. Due to the enormous computational cost posed by LES, very simple chemistry model (i.e., based on single conserved scalar - mixture fraction) was used in the study (Raman, et al. 2003).

The work described in this paper represents the first to make use of the MEPDF method for combustion applications using realistic combustion chemistry (i.e., with multiple reactive scalars). A Reynolds Averaged Navier Stokes (RANS) approach based computational fluid dynamics (CFD) modeling tool for performing turbulent combustion simulations that

require finite rate chemistry has been developed. The new modeling tool is based on the MEPDF methodology and combines the following: the direct quadrature method of moments or DQMOM (Marchisio and Fox, 2004); the interaction-by-exchange-with-the-mean (IEM) mixing model (Villermaux and Devillon, 1972); and realistic combustion chemistry, defined by a skeletal mechanism, augmented reduced mechanism based on quasi-steady state assumption, or a detailed mechanism. A pseudo time splitting scheme is adopted to solve the MEPDF equations; the reaction source terms are computed with a highly efficient and accurate in-situ adaptive tabulation (ISAT) algorithm (Pope, 1997, Tang et al, 2005). The new modeling tool was benchmarked against experimental data for a series of well-characterized bluff-body stabilized turbulent flames (Masri, et al., 1998), and applied to simulate a full scale industrial furnace with low NOx burner. A 19-species augmented reduced mechanism (Sung, et al. 1998) was used in these simulations.

The remainder of the paper is organized as follows. The mathematical model is described firstly, including multi-environment PDF model using direct quadrature method of moments and the implementation of radiation heat transfer model using discrete-ordinates method (DOM). The numerical solution method is discussed subsequently. The demonstration problems and simulation results are then presented in the next section, and conclusions are drawn in the final section.

Mathematical model

Multi-environment PDF model using direct quadrature method of moments

A brief introduction of the model is provided here. More detailed description about the model can be found elsewhere (Fox, 2003). The model development begins with a closed joint composition PDF transport equation:

$$\frac{\partial(\overline{\rho}f_\phi)}{\partial t} + \nabla \cdot (\overline{\rho}\,\overline{\mathbf{u}}f_\phi) - \nabla \cdot (\Gamma_e \nabla f_\phi) = -\frac{\partial}{\partial \psi_i}\left[\left(C_\phi \frac{\varepsilon}{k}(\langle\phi_i\rangle - \psi_i) + S_i(\psi)\right)f_\phi\right] \tag{1}$$

Note the IEM mixing model is used in Equation (1). This multi-dimensional equation is usually solved using a particle based Monte-Carlo scheme (see (Pope, 1985)), a method which is computationally too expensive for most combustion engineering applications - even with simple chemistry. In the MEPDF model, the joint PDF for N_s scalars is represented by multiple delta functions in the composition space, and is assumed to be of the form:

$$f_\phi(\psi; \mathbf{x}, t) = \sum_{n=1}^{N_e} p_n(\mathbf{x}, t)\prod_{\alpha=1}^{N_s} \delta[\psi_\alpha - \langle\phi_\alpha\rangle_n(\mathbf{x}, t)] \tag{2}$$

Using the direct quadrature method of moments (DQMOM) (Marchisio and Fox, 2004), a set of transport equations for weights $p_n(\mathbf{x}, t)$ and locations $\langle\phi_\alpha\rangle_n(\mathbf{x}, t)$ of the delta functions can be derived based on a pre-determined number of "environments", where each environment corresponds to a single delta-peak. The DQMOM equations are

$$\frac{\partial(\overline{\rho}p_n)}{\partial t} + \nabla \cdot (\overline{\rho}\,\overline{\mathbf{u}}p_n) - \nabla \cdot (\Gamma_e \nabla p_n) = \overline{\rho}a_n \tag{3}$$

$$\frac{\partial(\bar{\rho} p_n \langle \phi_\alpha \rangle_n)}{\partial t} + \nabla \cdot (\bar{\rho}\, \bar{\mathbf{u}} p_n \langle \phi_\alpha \rangle_n) - \nabla \cdot [\Gamma_e \nabla (p_n \langle \phi_\alpha \rangle_n)] = \bar{\rho} p_n \mathbf{S}_\alpha (\langle \phi \rangle_n) + \bar{\rho} b_{\alpha n} \tag{4}$$

where $\mathbf{S}_\alpha (\langle \phi \rangle_n)$ is the (closed) chemical source terms evaluated at node composition $\langle \phi \rangle_n$, and terms a_n and $b_{\alpha n}$ are to be determined using the DQMOM method, which ensures that the DQMOM equations match the moment equations of the scalar. Substituting Equation (2) into Equation (1) leads to

$$\sum_{n=1}^{N_e} \left[\delta(\psi - \langle \phi_\alpha \rangle_n) + \langle \phi_\alpha \rangle_n \delta^{(1)} (\psi - \langle \phi_\alpha \rangle_n) \right] a_n - \sum_{n=1}^{N_e} \delta^{(1)} (\psi - \langle \phi_\alpha \rangle_n) b_{\alpha n}^*$$

$$= \sum_{n=1}^{N_e} \delta^{(2)} (\psi - \langle \phi_\alpha \rangle_n) p_n c_{\alpha n} + R(\psi; \mathbf{x}, t) \tag{5}$$

where

$$c_{\alpha n} \equiv \Gamma_e (\nabla \langle \phi_\alpha \rangle_n)^2 \tag{6}$$

$$b_{\alpha n}^* = p_n S_\alpha (\langle \phi \rangle_n) + b_{\alpha n} \tag{7}$$

$R(\psi; \mathbf{x}, t)$ is the right-hand-side of Equation (1), and the derivatives of delta function are defined as in (Pope, 2000):

$$\int_{-\infty}^{+\infty} \delta^{(m)} (x - s) g(x) \mathrm{d}x = (-1)^m g^{(m)}(s) \tag{8}$$

The definition of a_n and $b_{\alpha n}$ is given by Equations (3) and (4). The only assumption made so far is that the shape of the PDF is approximated by a finite-set of delta functions. A set of $2N_e$ moments must be chosen in order to define a_n and $b_{\alpha n}^*$.

In this study, only the pure moments, namely the mean and variance of a scalar, are used to determine the source terms. For a two-environment case, one can arbitrarily set a_1 and a_2 to 0, and then use $m = 1, 2$ to calculate $b_{\alpha 1}^*$ and $b_{\alpha 2}^*$, which are given by:

$$b_{\alpha 1}^* = \frac{c_{\alpha 1} + c_{\alpha 2}}{\langle \phi_\alpha \rangle_1 - \langle \phi_\alpha \rangle_2} - \frac{1}{2} C_\phi \frac{\varepsilon}{k} p_1 p_2 (\langle \phi_\alpha \rangle_1 - \langle \phi_\alpha \rangle_2) + p_1 S_\alpha (\langle \phi \rangle_1) \tag{11}$$

and

$$b_{\alpha 2}^* = -\frac{c_{\alpha 1} + c_{\alpha 2}}{\langle \phi_\alpha \rangle_1 - \langle \phi_\alpha \rangle_2} + \frac{1}{2} C_\phi \frac{\varepsilon}{k} p_1 p_2 (\langle \phi_\alpha \rangle_1 - \langle \phi_\alpha \rangle_2) + p_2 S_\alpha (\langle \phi \rangle_2) \tag{12}$$

Thus:

$$b_{\alpha 1} = -b_{\alpha 2} = \frac{c_{\alpha 1} + c_{\alpha 2}}{\langle \phi_\alpha \rangle_1 - \langle \phi_\alpha \rangle_2} - \frac{1}{2} C_\phi \frac{\varepsilon}{k} p_1 p_2 (\langle \phi_\alpha \rangle_1 - \langle \phi_\alpha \rangle_2) \tag{13}$$

In determining the source terms, one of the important criteria is that the pre-multiplier of the **b** vector in Equation (13) is invertible. It should also be noted that a_n need not be set to zero and can be determined through a set of extended non-linear equations.

Implementation of Radiation Heat Transfer Model in MEPDF

Radiation is typically the most significant mode of heat transfer in practical combustion equipment. Accurately simulating radiation heat transfer to specific regions in a system requires a model that can account for both absorbing-emitting radiation processes and complex system geometries, including arbitrary structures such as convective tube passes. REI's model utilizes the discrete-ordinates method (DOM) that has proven to be a viable choice for modeling radiation in combustion systems, both in terms of computational efficiency and accuracy. The model has been implemented into the AMR flow solver and is modified to couple with the MEPDF solver.

The discrete-ordinates method solves the integral-differential radiation heat transfer equation (RTE) in a number of discrete angular directions spanning the total solid angle of 4π steradians. The discrete-ordinates representation of the mean radiation heat transfer equation can be written in Cartesian coordinates as

$$\mu_m \frac{\partial \langle I_m \rangle}{\partial x} + \eta_m \frac{\partial \langle I_m \rangle}{\partial y} + \xi_m \frac{\partial \langle I_m \rangle}{\partial z} = -\langle k_{ag} \rangle \langle I_m \rangle + \langle e_{bg} \rangle \tag{14}$$

$\langle e_{bg} \rangle$ is the mean gas blackbody radiation intensity, which can be calculated as

$$e_{bg} = \frac{\sigma}{\pi} k_{ag} T_g^{\,4} \tag{15}$$

The radiation heat loss rate per unit volume that forms the radiation source term in the energy transport equation can be expressed as

$$Q_r = \nabla \cdot \mathbf{q} = 4\pi e_{bg} - k_{ag} \sum_{m=1}^{M} w_m I_m \tag{16}$$

The radiation term in the PDF equation can be expressed as, after combining with Equation (16),

$$\frac{\partial}{\partial \psi_h} \left[\left\langle \left(4\sigma k_{ag} T_g^{\,4} - k_{ag} \sum_{m=1}^{M} w_m I_m \right) \middle| \boldsymbol{\psi} \right\rangle f_\varphi \right] = \frac{\partial}{\partial \psi_h} \left[4\sigma \langle k_{ag} T_g^{\,4} \rangle f_\varphi \right] - \frac{\partial}{\partial \psi_h} \left[\left\langle \left(k_{ag} \sum_{m=1}^{M} w_m I_m \right) \middle| \boldsymbol{\psi} \right\rangle f_\varphi \right] \tag{17}$$

The first term on the right-hand side of equation (17) represents radiative emission and appears in closed form because the conditional mean can be calculated from local composition exactly. The second term on the right-hand side of equation (17) needs to be modeled. The model adopted here is the optically thin eddy approximation that suggests that the local incident radiation intensity I_m is only weakly correlated to the local radiative properties. This leads to

$$\frac{\partial}{\partial \psi_h} \left[\left\langle \left(k_{ag} \sum_{m=1}^{M} w_m I_m \right) \middle| \boldsymbol{\psi} \right\rangle f_\varphi \right] \approx \frac{\partial}{\partial \psi_h} \left[\left(k_{ag} \sum_{m=1}^{M} w_m \langle I_m \rangle \right) f_\varphi \right] \tag{18}$$

Equation (18) can be coupled with equation (14) to solve for the change in enthalpy in each environment due to radiation and hence the mean temperature field.

Numerical Solution Schemes

A separate MEPDF solver for Equations (3) and (4) has been developed and coupled with REI's 3D, multi-block flow solver, which employs a non-staggered body-fitted grid. A pressure-based scheme (Patankar, 1980) is employed to solve the momentum and continuity equations. An Algebraic Multi-grid (AMG) method is used to accelerate convergence of the pressure equation. All equations are discretized using a finite volume method. For momentum and scalar equations a second-order Total Variation Diminishing (TVD) scheme is applied. The highly nonlinear chemical source terms on the right-hand-side of Equation (4) require special treatment to achieve quick convergence of the solutions. A time-splitting scheme is used to solve Equations (3) and (4). The ISAT algorithm is applied in order to speedup the integration of the chemical source terms.

Time-splitting schemes are widely used for Monte-Carlo PDF methods for turbulent reacting flow simulations where the chemical source terms, micro-mixing, convective and dissipation terms are integrated in separate sub-time-steps (Tang *et al.*, 2000). Equations (3) and (4) can be re-written as:

$$\frac{\partial \varphi}{\partial t} = L(\varphi; \mathbf{x}, t) + \mathbf{S}(\varphi) \tag{19}$$

where $\varphi = [p_1, \ldots, p_n, \langle \phi_1 \rangle_1, \ldots, \langle \phi_{Ns} \rangle_1, \ldots\ldots, \langle \phi_1 \rangle_{Ne}, \ldots, \langle \phi_{Ns} \rangle_{Ne}]^T$ is the array of unknown scalars, $\mathbf{S}(\varphi)$ is the chemical source terms, and $L(\varphi; \mathbf{x}, t)$ represents all other terms including convection, diffusion, and micro-mixing, etc. The time-splitting scheme to integrate Equation (19) is described as follows:

Step 1: $\qquad \varphi^* = \varphi^n + \int_0^{0.5\Delta t} S(\varphi)\,\mathrm{d}t, \qquad \varphi = \varphi^n \quad \text{at} \quad t = 0$

Step 2: $\qquad \varphi^{**} = \varphi^* + \int_0^{\Delta t} L(\varphi; \mathbf{x}, t)\,\mathrm{d}t, \qquad \varphi = \varphi^* \quad \text{at} \quad t = 0$

Step 3: $\qquad \varphi^{n+1} = \varphi^{**} + \int_0^{0.5\Delta t} S(\varphi)\,\mathrm{d}t, \qquad \varphi = \varphi^{**} \quad \text{at} \quad t = 0$

The time accuracy of the above scheme is second-order. Because only the steady state solution is of interest at present, local time stepping is used to accelerate convergence. The integration of the chemical source terms in a separate time step allows us to utilize the ISAT algorithm to tabulate the solutions of the chemical source term integration.

The idea of ISAT is to avoid performing expensive chemistry calculations in every grid cell at every iteration, but instead to store the information from many fewer calculations, and then (when possible with sufficient accuracy) to retrieve the information. An ISAT algorithm, which features several new strategies that significantly improves the efficiency over the original algorithm proposed by Pope (1997), has been used in this research.

The coupling of the scalar solver and the flow solver is described as follows:

1) Solve for the mean velocity, pressure and turbulent kinetic energy and dissipation rate fields using the flow solver;

2) Integrate the scalar transport equations for one time step using fixed velocity and turbulent diffusivity;

3) Update the gas properties (density, viscosity, etc.) based on the new scalar fields;

4) Step 1, 2, and 3 are repeated until both flow and scalar fields are converged.

This method can be extended to time dependent turbulent reacting flow calculations in a straightforward manner by modifying the flow solver to use time-accurate calculations.

When solving Equation (3) and (4), the correction source terms $b_{\alpha n}$ need special treatment. For a two-environment model, these terms are computed by Equation (13). As can be seen, for Equation (13) to be valid, the two delta peaks in the composition space must be independent, i.e., $\langle \phi_\alpha \rangle_1 \neq \langle \phi_\alpha \rangle_2$, which is not guaranteed when deriving the system of equations. Several methods have been suggested to deal with the situation where the two delta functions approach each other or crossover (Wang and Fox, 2003). We found the following approach to be very effective and robust for all the cases studied, and to have minimum impact on the results. For each cell in the calculation domain, $b_{\alpha n}$ is limited by

$$\left| b_{\alpha n} \right| \leq \max\left[c_1 \sum A_{nb} \cdot (d\phi_\alpha)_{\max}, \quad c_2 S_{mixing} \right] \tag{20}$$

where A_{nb} are the neighbor coefficients in the discretized equation; $(d\phi_\alpha)_{\max}$ is the maximum change in species mass fractions among neighboring cells; and S_{mixing} is the magnitude of the mixing source term. c_1 and c_2 are constants set to 0.2 and 10, respectively.

Demonstration problems and simulation results

Demonstration problem – Sydney bluff-body flames

Masri et al. (1998) and Dally et al. (1998) have performed a series of systematic experiments to investigate bluff body stabilized flames. The bluff-body burner provides a flame suitable for the study of turbulence-chemistry interactions. Bluff-body burners also bear a great similarity to practical combustors used in many industrial applications. This geometry is, therefore, a suitable compromise as a model problem because it has some of the complications associated with practical combustors while preserving relatively simple and well-defined boundary conditions.

The burner is centered in a co-flowing stream of air and generally consists of a circular bluff-body with an orifice at its center for the main fuel. A complex flow pattern forms

downstream of the face of the bluff-body where a recirculation zone is formed to produce enough hot gases to stabilize the flame to the burner. At sufficiently high fuel velocity, the jet flow penetrates through the recirculation zone and forms a jet-like flame further downstream.

Methane (CH_4), ethylene (C_2H_4), propane (C_3H_8), and their mixture with H_2 and CO were used as fuels. The velocity fields were measured by Laser Doppler Velocimetry (LDV) and scalar fields were measured by single-point Raman-Raleigh-Laser Induced Fluorescence (LIF). In this work, we use the Methane-Hydrogen flames as the test problem. The fuel for the flames is a mixture of hydrogen and methane in volume ratio 1:1. The jet bulk velocities for these flames range from 118m/s to 214m/s. Experimental data for both non-reactive (cold flow) case and reactive case of these flames are available. Velocity field data include mean axial velocity, radial velocity and their variances. For the cold flow, the scalar field data consist of the mean and variance of mixture fraction. For the reactive case, the scalar field data consist of means and variances of mixture fraction, temperature and some major and minor species. These species include O_2, N_2, H_2, H_2O, CO, CO_2, CH_4, OH, and NO, etc.

Shown in Figure 1 is the computational mesh used in the simulations. The dimensions of the computational domain are $7D_B$ in axial direction and $3D_B$ in radial direction, where D_b is the bluff-body diameter. The mesh size is 141×161. Note that a short length (1 cm) of the bluff-body and fuel nozzle is included in the computational domain. Uniform velocity profiles were specified for both co-flowing air stream and fuel jet at the inflow boundary. At the centerline, symmetry boundary conditions are given for all variables except radial velocity component, which is 0 at the axis. Slip wall boundary conditions are given at the top boundary of the computational domain. The bluff body is assumed to be adiabatic.
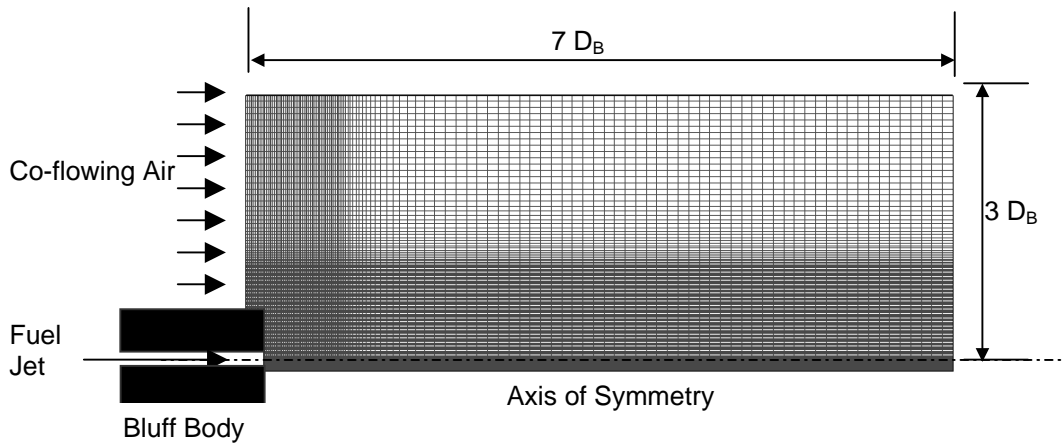

Figure 1. Sketch of the computational domain

The inflow boundary conditions for the MEPDF model require careful treatment. For a two-environment model using a detailed chemical kinetic mechanism, there are $2n_s + 3$ scalars need to be solved in the MEPDF model, namely the weight function p_1, $G_{1i} = p_1 Y_i, i = 1, \ldots, n_s$, and $H_1 = p_1 h_1$ in environment 1, and $G_{2i} = p_1 Y_i, i = 1, \ldots, n_s$, and $H_2 = p_2 h_2$ in environment 2,

where $p_2 = 1 - p_1$, n_s is the number of species, Y_i is the mass fraction of species *i*, and h_1, h_2 are specific enthalpy in each environment. The inlet conditions in the fuel inlet stream are $p_1 = 1.0$, $G_{1i} = Y_i^{fuel}, i = 1, \ldots, n_s$, $H_1 = h_1^{fuel}$, $G_{2i} = 0.0, i = 1, \ldots, n_s$, and $H_2 = 0.0$; and in the air inlet stream are $G_{1i} = 0, i = 1, \ldots, n_s$, $H_1 = 0.0$, $G_{2i} = Y_i^{air}, i = 1, \ldots, n_s$, and $H_2 = h_1^{air}$, where Y_i^{fuel} and Y_i^{air} are the mass fraction of species *i* in the co-flowing air and in fuel jet, respectively. The same rule applies to h_1^{fuel} and h_1^{fuel} .

A 19-species 12-step augmented reduced mechanism (Sung, *et al.* 2001) derived from the GRI 2.11 mechanism (Bowman, *et al.*) for methane oxidation is used in the calculations of these bluff-body flames.

Presented here are simulation results of two bluff-body flames, where the velocity of the air stream is kept at 40 m/s while the velocity of the fuel jet is 118 m/s and 214 m/s for flame HM1 and flame HM3, respectively. The bottom row of Figures 2-4 shows the calculated radial profiles of mean temperature, and the mass fractions of CO and NO, respectively, at three axial locations. Simulation results extracted from a stand-alone joint velocity-turbulence frequency-composition PDF method (Liu, *et al.* 2005) are shown in the top row for comparison purposes.
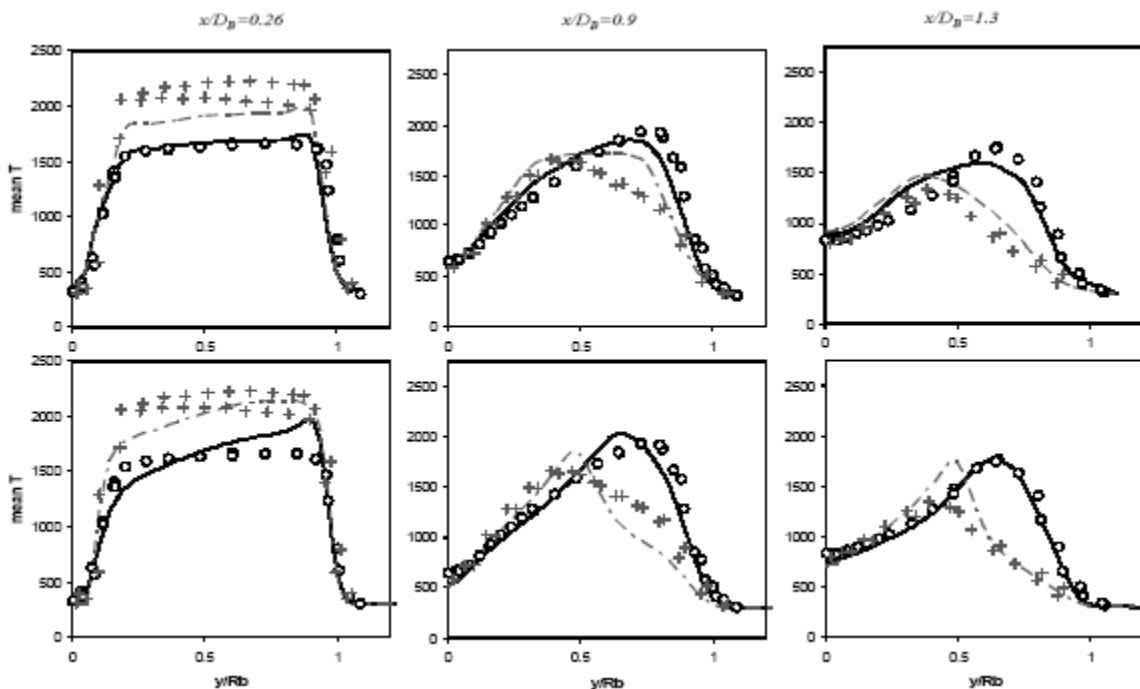

Figure 2. Radial profiles of the mean temperature. Circles: experiments, solid lines: simulations for flame HM1; pluses: experiments, dash-dotted lines: simulations for flame HM3. Top row: transport PDF; bottom row: MEPDF.
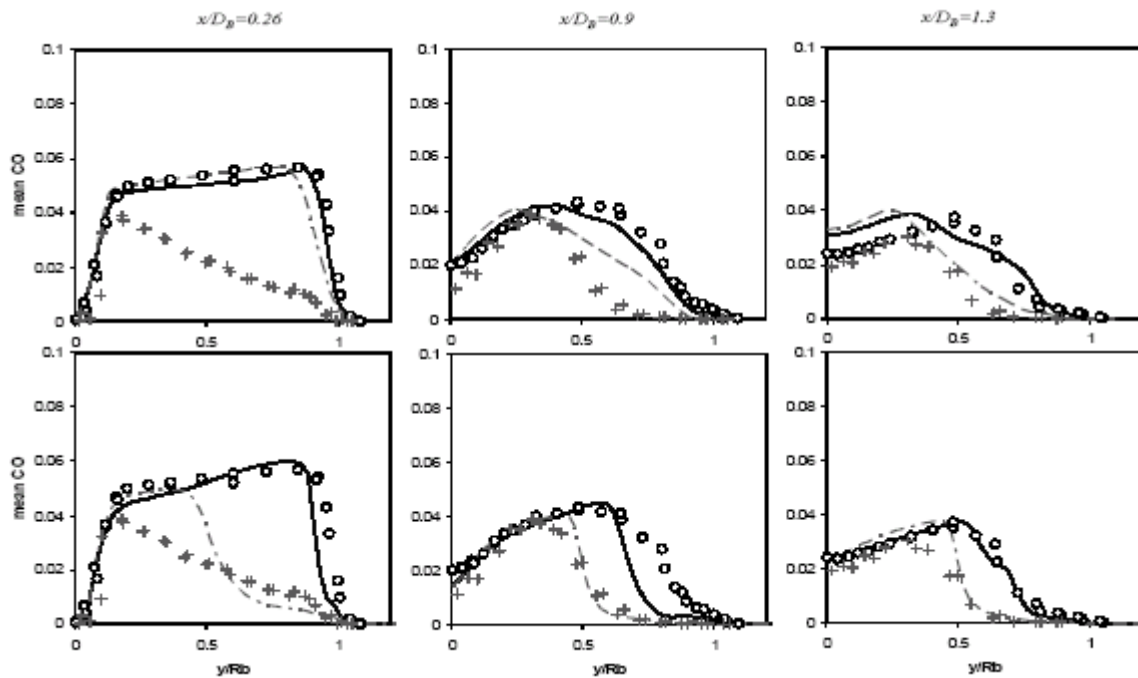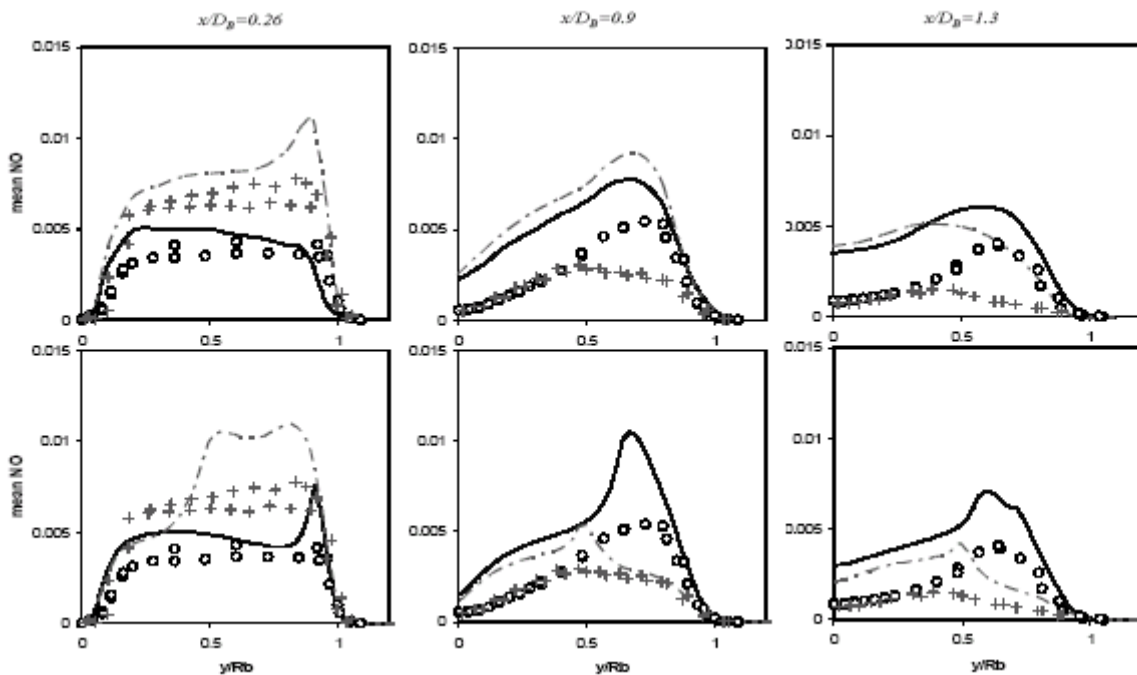
Figure 3. Radial profiles of the mean mass fraction of CO. Circles: experiments, solid lines: simulations for flame HM1; pluses: experiments, dash-dotted lines: simulations for flame HM3. Top row: transport PDF; bottom row: MEPDF.

Figure 4. Radial profiles of the mean mass fraction of NO. Circles: experiments, solid lines: simulations for flame HM1; pluses: experiments, dash-dotted lines: simulations for flame HM3. Top row: transport PDF; bottom row: MEPDF.

For flame HM1, the predicted and measured temperature profiles are in good agreement. The profiles of CO mass fraction also agree very well with the data, except for the fuel lean side at x/D=0.9 where the CO mass fraction is under-predicted. The NO mass fraction is over-predicted by 10 to 30%. Similar observations can be made on the HM3 simulation using the MEPDF method. Overall, the trends exhibited in these two very different flames (i.e., one with low jet velocity and near equilibrium, one with a high jet velocity and near global extinction) are well predicted by the MEPDF model. This highlights the capability of the new tool to accurately capture a broad range of combustion conditions.

From Figures 2-4, it can be seen that the levels of accuracy in the simulations using the joint PDF approach and the MEPDF approach are comparable. The MEPDF does a better job in predicting the trends found in these flames than does the joint PDF method. For example, the joint PDF calculations completely miss the trend of the CO mass fractions at x/D=0.26 and the trend of the NO mass fractions at x/D=0.9, while the MEPDF calculations successfully captures the trend. The 3-D MEPDF simulations required only about 12h of CPU time to converge on a 2.4-GHz Opteron workstation. The joint PDF simulations required about 400h of CPU time on a similar computer (Liu *et al*, 2005). Therefore for this example we conclude that the MEPDF model provides an improved prediction but at a significantly reduced computational cost.

Demonstration problem – Single burner test furnace

The MEPDF model has also been used to simulate a single burner test furnace (SBTF) based on an actual Performance Demonstration. The purpose of the SBTF is to provide a test bed for low NO_x gas burners commonly used in process heaters. The SBTF provides a means to study the impact of different firing conditions on burner performance. In addition, the SBTF results can be used to assist in modeling the burner conditions in full sized process heater furnaces containing a large number of burners.

Due to the symmetric location of the burner in the furnace, only half of the furnace was modeled (see Figure 5.1 (a)). Some details of the low NO_x burner are shown in Figure 5.1 (b) and (c), where the burner wall surface is colored by calculated wall temperature. The SBTF consists of a rectangular furnace with one up-fired burner located on the furnace floor along one wall (Figure 5.1 (a)). The burner is a natural draft (single fuel) gas burner. The burner consists of eight gas tips: 3 so-called primary tips are mounted inside the throat of the burner tile, close to the centerline; 3 so-called staged gas tips are positioned outside the side of the tile and fire up the outside of the angled front of the tile; and 2 additional primary gas tips are positioned outside the tile at each end firing mainly horizontally through an aperture in the tile into the air stream flowing up through the throat of the tile. Each gas tip consists of several minute gas jets, each oriented so as to enhance fuel-air mixing and to re-circulate flue gas as a mechanism for NO_x reduction. The furnace also contains five partially insulated, water-cooled tubes located along the furnace wall opposite the burner (three of them are shown in Figure 5.1 (a)). The furnace has a circular exit located approximately at the center of the furnace (the blue area shown in Figure 5.1 (a)).
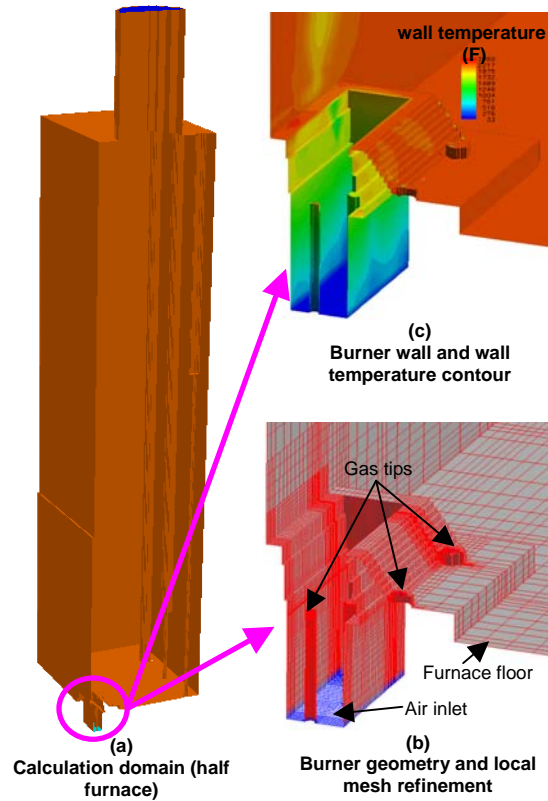
Figure 5. SBTF calculation domain
and mesh refinement.

The dimensions of the calculation domain are approximately 2.0 m in width, 1.75 m in depth, and 10.0 m in height. The base grid is $34 \times 36 \times 77$. To resolve the smallest fuel jet nozzle nine levels of local mesh refinements are applied; hence, the inlet flow area of each jet contains at least 10×10 cells. Mesh refinement is also used to resolve the process heater tube geometries. To better represent the intense turbulent mixing of the primary fuel jets and air flow, and the staged fuel jets and the flue gas, three levels of manual mesh refinements are applied to the cells inside the burner well and above the staged gas tips. The total number of cells after mesh refinement is about 250 K.

The simulated case was a normal firing rate of 7.5 MMBtu/hr (2.2 MW). In the test, the burner fired a mixture of 40mol% hydrogen and 60 mol% methane. The fuel mass flow rate is about 0.04 kg/sec and the air mass flow rate is about 0.8 kg/sec. The excess oxygen is about 2.1 mol% (dry basis). Both the fuel flow and the air flow are at a temperature of 283.15 K.

Preliminary results of the MEPDF simulations are compared with the results from two other combustion models. The first one uses a traditional assumed shape PDF model and equilibrium chemistry determined by mixture fraction and is referred to as EQ. The second one uses a joint composition transport PDF model with finite rate chemistry and is referred to as PDF. The simulation using the MEPDF model and the EQ chemistry model is referred to as MEPDF-EQ, where the mixture fraction in each environment is solved and used to compute the equilibrium compositions in each environment. The simulation using the MEPDF model and finite rate chemistry is referred to as MEPDF-FR, where the same model has been used to model the bluff-body flames. A 19 species reduced mechanism is used in both the PDF and the MEPDF-FR simulations. Figure 6 shows the comparison of the gas temperature contours at the symmetry plane. Comparisons of the species concentration at the model outlet and of the simulation run time are listed in Table 1.
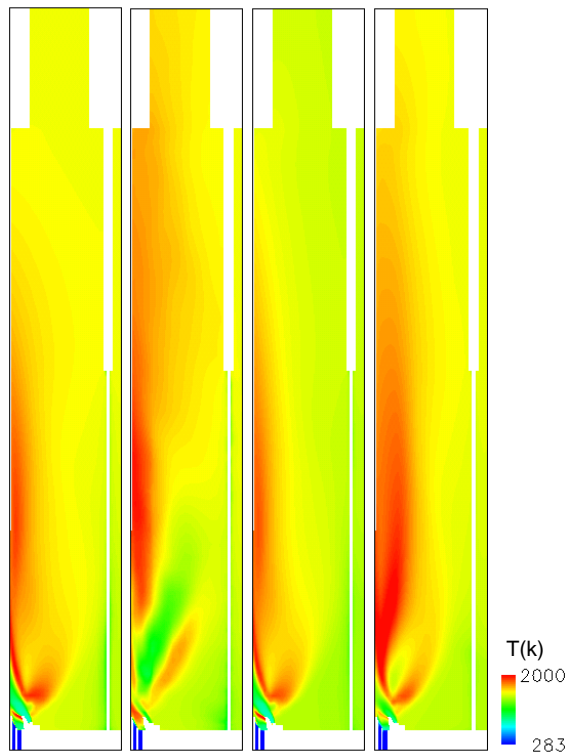

Figure 7. Temperature contours at symmetry plane.
From left to right: EQ, PDF, MEPDF-EQ, and MEPDF-FR

It can be seen in Figure 7 that the flame shapes predicted by the PDF model and the MEPDF-FR model are similar to each other while quite different from the flames predicted by the two models using equilibrium chemistry. With finite rate chemistry, the predicted flames are broader and longer and seem more distributed than the flames predicted using an equilibrium chemistry model.

Table 1. Comparison between measured and predicted quantities
and CPU time among simulations

	Outlet NO (ppm)	Outlet CO (ppm)	CPU time
Measurements	53	1	N/A
EQ	534	0	~2 days, single CPU
PDF	50	9	~ 60 days, four CPU
MEPDF-EQ	332	4	~ 3 days, single CPU
MEPDF-FR	102	9	~ 15 days, single CPU

Compared to the experimental measurements, the transport PDF model achieves the best result for predicting NO concentration. The MEPDF-FR model over-predicts NO by a factor of one, which is consistent with the results seen in the bluff-body flame simulation described in the previous section. The two models assuming equilibrium chemistry are not adequate for NO prediction, although the MEPDF-EQ result shows improvement. In terms of CO prediction, the models using equilibrium chemistry do a better job than do the two models using finite rate chemistry described by the 19 species reduced mechanism.

The transport PDF method gives better NO prediction than does MEPDF-FR because it uses a large number of notional particles (i.e., 20 particles per cell), which may provide a more accurate representation of the highly nonlinear chemical source terms. The chemical source terms are only represented by two environments in the MEPDF-FR approach used in the simulation of the test furnace. The CPU time spent in the MEPDF-FR simulation is only 6% of that spent in the PDF simulation.

Conclusions

Originally developed by the chemical engineering community to model simple chemical reaction processes (e.g., mixing tanks), the work described here represents the first to make use of the MEPDF method for combustion applications using realistic combustion chemistry. A CFD modeling tool has been developed which incorporates the MEPDF model into REI's three-dimensional turbulent flow solver. The new modeling tool has been benchmarked against other numerical solutions and experimental data for a series of well-characterized bluff-body stabilized turbulent flames, and has been applied to simulate a full scale industrial single burner test furnace.

Overall, we believe that the trade-off (i.e., accuracy vs. efficiency) between the transport PDF method and the MEPDF method is dependent on the application. Whether or not the MEPDF method will work satisfactorily for more complex flames is still an open question. Nevertheless, its ease of implementation and the advantages it offers over simply neglecting the sub-grid scale fluctuations makes it an attractive CFD tool for modeling practical combustion devices.

Acknowledgements

References

Barlow, R.S., *International Workshop on Measurement and Computation of Turbulent Nonpremixed Flames*, http://www.ca.sandia.gov/TNF

Bilger, R.W., (1993), Conditional Moment Closure for Turbulent Reacting Flow, *Physics of Fluids*, 5(2):436-444.

Bockelie, M., Swensen, D., Denison, M., Montgomery, G., and Pernice, M., (2000), *SIAM Computational Sciences and Engineering Conference 2000*.

Bowman, C.T., Hanson, R.K., Davidson, D.F., Gardiner, Jr.., E.C., Lissianski, V., Smith, G.P., Golden, D.M., Frenklach, M., and Glodenburg, M., http://www.me.berkeley.edu/gri_mech/

Brown, D.J., (2004), *AFRC-JFRC Joint International Combustion Symposium 2004*.

Brown, D.J., (2005), *AIChE Spring Meeting*, Atlanta.

Dally, B.B., Marsi, A,R., Barlow, R.S., and Fiechtner, G.J., (1998), *Combust. Flame*, 114:119.

Fox, R.O., (2003), "Computational Models for Turbulent Reacting Flows", Cambridge University Press.

Lindstedt, R.P., Louloudi, S.A., and Vaos, E.M., (2000), *Proc. Combust. Inst.*, 28:149-156.

Liu, K. and Pope, S.B., (2005), *Combust. Flame* 141:89-117.

Marchisio, D.L. and Fox, R,O., (2004), *Journal of Aerosol Science*.

Masri, A.R., http://www.mesh.eng.usyd.edu.au/research/energy/#data, *The University of Sydney and The Combustion Research Facility, Sandia National Laboratories*.

Masri, A.R., Kelman, J.B., and Dally, B.B., (1998), *Proc. Combust. Inst.*, 27:1031.

Patankar V.S., (1980), Numerical Heat Transfer and Fluid Flow, Hemisphere Publishing Corporation, New York.

Peters, N., (1984), *Prog. Energy Combust. Sci.,* 10:319-339.

Pope, S.B., (1985), *Prog. Energy Combust. Sci.*, 11:119-192.

Pope, S.B., (1997), *Combust. Theo. Modelling*, 1:41-63.

Raman, V., Fox, R.O., and Harvey, A.D., (2004), *Combustion and Flame*, 136:327.

Raman, V., Pitsch, H., and Fox, R.O., (2003), *Annual Research Briefs*, Center for Turbulence Research.

Sung, C.J., Law, C.K., and Chen, J-Y., (2001), *Combust. Flame* 125(1-2):906-919.

Tang, Q., Xu, J., and Pope, S.B., (2000), *Proc. Combust Inst.*, 28:133-139.

Villermaux, J. and Devillon, J.C., (1972), *Proceedings of the 2nd International Symposium on Chemical Reaction Engineering*, New York, Elsevier.

Wang, L. and Fox, R.O., (2004), *AIChE Journal*, 2004.

Xu, J. and Pope, S.B., (2000), *Combust. Flame*, 123:281.